SLAC – PUB – 4323
May 1987
(T/E)

TESTING QUANTUM CHROMODYNAMICS IN ELECTROPRODUCTION*

STANLEY J. BRODSKY

Stanford Linear Accelerator Center
Stanford University, Stanford, California 94305

Introduction

Deep inelastic lepton nucleon scattering has been one of the key testing grounds of QCD over the past two decades. Measurements of the nucleon and nuclear structure functions have not only tested the short-distance properties of the theory, (such as the scaling properties of structure functions and their logarithmic evolution with momentum transfer), but they have also illuminated the nonperturbative bound state structure of the nucleon and nuclei in terms of their quark and gluon degrees of freedom. For the most part, this information has been obtained from single-arm inclusive experiments where only the recoil lepton was detected.

One of the important potential advantages of an internal target facility in an electron storage ring as discussed in this workshop is that the entire final state of electroproduction can be measured in coincidence with the scattered electron with close to 4π acceptance. In the case of the PEP ring ($E(e^{\pm}) \sim 15$ GeV), measurements can be performed above the onset of Bjorken scaling. Both polarized and unpolarized hydrogen and nuclear targets may be feasible, and eventually even polarized electron beams may be available. High precision comparisons between electron and positron scattering would allow the study of higher order QED and electroweak interference effects. The asymmetry in the cross sections for $e^{\pm}p \to e^{\pm}\gamma X$ can be sizeable,[1] providing a sum rule for the cube of the charges of the quarks in the target.

At the most basic level, Bjorken scaling of deep inelastic structure functions implies the production of a single quark jet, recoiling against the scattered lepton. The spectator system–the remnant of the target remaining after the scattered quark is removed–is a colored $\bar{3}$ system. (See fig. 1.) According to QCD factorization, the recoiling quark jet, together with the gluonic radiation produced in the scattering process, produces hadrons in a universal way, independent of the target or particular hard scattering reaction. This jet should be identical to the light quark jets produced in e^+e^- annihilation. In contrast, the hadronization of the spectator system depends in detail on the target properties. Unlike the quark jet, the leading particles of the target spectator system do not evolve and thus should not depend on the momentum transfer Q^2 [at fixed $W^2 = (q+p)^2$]. At present we do not have a basic understanding of the physics of hadronization, although phenomenological approaches, such as the Lund string model, have been successful in parameterizing many features of the data.

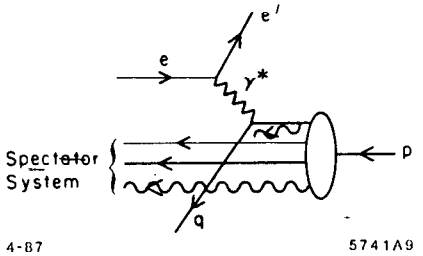

Fig. 1. Struck quark and spectator systems in electroproduction.

At a more detailed level, the features of the standard leading twist description are modified by coherent or nonperturbative effects. For example, higher twist–power-law suppressed contributions arise when two or more quarks recoil against the scattered lepton. At high energies, the quark jet does not change its state or hadronize over a distance scale proportional to its energy. Thus inelastic or absorptive processes cannot occur inside a nucleus–at least for the very fast hadronic fragments. We will discuss this target length condition[2,3] in more detail below. Nevertheless, a nuclear target can provide an essential tool for studying the detailed features of jet hadronization since the fast fragments are expected to scatter elastically in the nuclear medium, and the slow particles can interact inelastically and shower inside the nucleus. A review of the QCD predictions for jet hadronization can be found in Berger's contribution[4] to this workshop.

Many of the novel features expected in QCD are also apparent in QED. It is thus often useful to keep a QED analog in mind, replacing the target by a neutral atom such as positronium. Even in QED where there is no confinement, one expects in certain kinematic regions significant corrections to the Bjorken scaling associated with positron or electron knockout, in addition to the logarithmic evolution of the QED structure functions associated with induced photon radiation. For example, at low Q^2, the interference between amplitudes where different constituents are struck become important. Near threshold, where charged particles emerge at low relative velocities, there are strong Coulomb distortions, as summarized by the Sommerfeld[5] factor. In QCD these have their analog in a phenomena called "jet coalescence"[6] which we discuss in a later section. The Coulomb distortion factor must be included if one wants to maintain duality between the inelastic continuum and a summation over exclusive channels in electroproduction.

My main emphasis is this talk, however, is in the study of exclusive channels in electroproduction. It is clearly interesting to study how the summation of such channels yields the total inelastic cross section. More important, each individual exclusive channel can provide detailed information on basic scattering mechanisms in QCD and how the scattered quarks and gluons recombine into hadrons. In certain cases such as Compton scattering and meson electroproduction, we can study new aspects of the light cone expansion for the product of two currents, thus extending the renormalization group analysis into a new domain.[7] The diffractive production of vector mesons at high Q^2 can test the basic composition of the Pomeron in QCD. Further, as we discuss in the next section, measuring exclusive reactions inside a nuclear target allows the study of "color transparency",[8,9] the "formation zone",[2] and other novel aspects of QCD.

Exclusive Channels in Electroproduction

In high momentum transfer inclusive reactions, the underlying quark and gluon scattering processes lead directly to jet production in the final state, To leading order in $1/Q^2$, the cross sections and jet hadronization can be understood at the probabilistic level. In contrast, in *exclusive* electroproduction processes, one studies quark and gluon scattering and their reformation into hadrons at the *amplitude* level. Exclusive reactions thus depend in detail on the composition of the hadron wavefunctions themselves.

* Work supported by the Department of Energy, contract DE-AC03-76SF00515.

Presented at the NPAS Workshop on Electronuclear Physics with Internal Targets, Stanford, California, January 5-8, 1987

There is now an extensive literature, both experimental and theoretical, describing the features of large momentum transfer exclusive reactions. The QCD predictions are based on a factorization theorem[10-14] which separates the nonperturbative physics of the hadron bound states from the hard scattering amplitude which controls the scattering of the constituent quarks and gluons from the initial to final directions. This is illustrated for the proton form factor in fig. 2. Electroproduction of exclusive channels provides one of the most valuable testing ground of this QCD formalism, since the incoming photon provides a probe of variable spacelike mass directly coupling to the hard-scattering amplitude.

It has been known since 1970 that a theory with underlying scale-invariant quark-quark interactions leads to dimensional counting rules[15] for large momentum transfer exclusive processes; e.g. $F(Q^2) \sim (Q^2)^{1-n}$ where n is the minimum number of quark fields in the hadron. QCD is such a theory; the factorization formula leads to nucleon form factors of the form:[16]

$$G_M(Q^2) = \left[\frac{\alpha_s(Q^2)}{Q^2}\right]^2 \sum_{n,m} a_{nm} \left(ln\ \frac{Q^2}{\Lambda^2}\right)^{-\gamma_n-\gamma_m} \times \left[1 + O(\alpha_s(Q)) + O\left(\frac{1}{Q}\right)\right]$$

The first factor, in agreement with the quark counting rule, is due to the hard scattering of the three valence quarks from the initial to final nucleon direction. Higher Fock states lead to form factor contributions of successively higher order in $1/Q^2$. The logarithmic corrections derive from an evolution equation[10,16] for the nucleon distribution amplitude. The γ_n are the computed anomalous dimensions, reflecting the short distance scaling of three-quark composite operators. The results hold for any baryon to baryon vector or axial vector transition amplitude that conserves the baryon helicity. Helicity non-conserving form factors should fall as an additional power of $1/Q^2$. Measurements of the transition form factor to the $J = 3/2$ $N(1520)$ nucleon resonance are consistent with $J_z = \pm 1/2$ dominance, as predicted by the helicity conservation rule.[17] It is very important to explicitly verify that $F_2(Q^2)/F_1(Q^2)$ decreases at large Q^2. The angular distribution decay of the $J/\Psi \to p\bar{p}$ is consistent with the QCD prediction $\lambda_p + \lambda_{\bar{p}} = 0$.

The normalization constants a_{nm} in the QCD prediction for G_M can be evaluated from moments of the nucleon's distribution amplitude $\phi(x_i, Q)$. There are extensive on-going theoretical efforts computing constraints on this nonperturbative input directly from QCD. The pioneering QCD sum rule analysis of Chernyak and Zhitnitskii[12] provides constraints on the first few moments of $\phi(x, Q)$. Using as a basis the polynomials which are eigenstates of the nucleon evolution equation, one gets a model representation of the nucleon distribution amplitude, as well as its evolution with the momentum transfer scale.

The QCD sum rule analysis predicts a surprising feature: strong flavor asymmetry in the nucleon's momentum distribution. The computed moments of the distribution amplitude imply that 65% of the proton's momentum in its 3-quark valence state is carried by the u-quark which has the same helicity as the parent hadron. (See fig. 3.) A recent comprehensive re-analysis by King and Sachrajda[18] has now confirmed the Chernyak and Zhitnitskii form in its essential details. In addition, Dziembowski and Mankiewicz[19] have recently shown that the asymmetric form of the CZ distribution amplitude can apparently be derived from a rotationally-invariant CM wavefunction transformed to the light cone using a Melosh-type boost of the quark spinors. The transverse size of the valence wavefunction is found to be significantly smaller than the mean radius of the proton–averaged over all Fock states. This was predicted in ref. 10. Dziembowski and Mankiewicz also show that the perturbative QCD contribution to the form factors dominates over the soft contribution (obtained by convoluting the non-perturbative wave functions) at a scale $Q/N \approx 1$ GeV, where N is the number of valence constituents. Similar criteria were also derived in ref. 20. Results of the similar Jacob and Kisslinger[21] analysis of the pion form factor are shown in fig. 4. Claims[22] that a simple overlap of soft hadron wavefunctions could fit the form factor data were based on wavefunctions which violate rotational symmetry in the CM.

A detailed phenomenological analysis of the nucleon form factors for different shapes of the distribution amplitudes has been given by Ji, Sill, and Lombard-Nelsen.[23] Their results show that the CZ wavefunction is consistent with the sign and

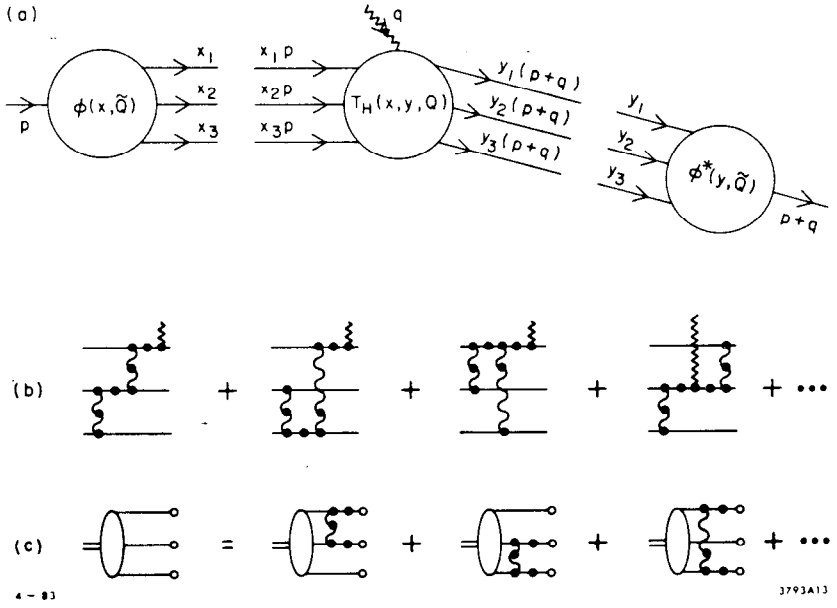

Fig. 2. Factorization of the nucleon form factor at large Q^2 in QCD.

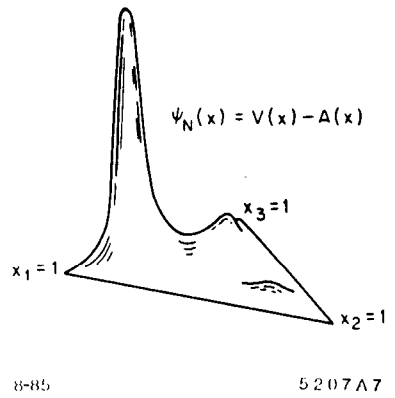

Fig. 3. QCD sum rule prediction for the proton distribution amplitude.

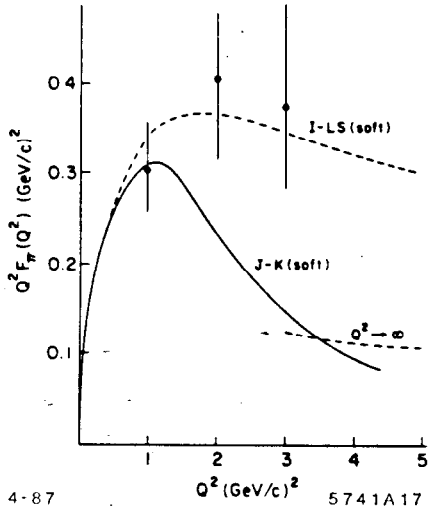

Fig. 4. Models for the "soft" contribution to the pion form factor. The Isgur-Llewellyn-Smith prediction[22] is based on a wavefunction with Gaussian fall-off in transverse momentum but power-law falloff at large x. The Jacob-Kisslinger prediction[21] is based on a rotationally symmetric form in the center of mass frame. The perturbative QCD contribution calculated with CZ[12] distribution amplitudes is consistent with the normalization and shape of the data for $Q^2 > 1$ GeV^2.

magnitude of the proton form factor at large Q^2 as recently measured by the American University/SLAC collaboration.[24] (See fig. 5.) The fact that the correct normalization emerges is a non-trivial test of the distribution amplitude shape; for example, the if the proton wavefunction has a non-relativistic shape peaked at $x_i \sim 1/3$ then one obtains the wrong sign for the nucleon form factor. Furthermore symmetrical distribution amplitudes predict a much too small magnitude for $Q^4 G_M^p(Q^2)$ at large Q^2. Gari and Stefannis[25] have developed a useful model for the nucleon form factors which incorporates the CZ distribution amplitude predictions at high Q^2 together with VMD constraints at low Q^2. Their analysis predicts sizeable values for the neutron electric form factor at intermediate values of Q^2. (See fig. 6.)

Measurements of the two-photon exclusive processes $\gamma\gamma \to \pi^+\pi^-$ and K^+K^- are in excellent agreement with the perturbative QCD predictions. The data[26] (see fig. 7) extend out to invariant mass squared 10 GeV^2, a region well beyond any significant contribution from soft contributions.

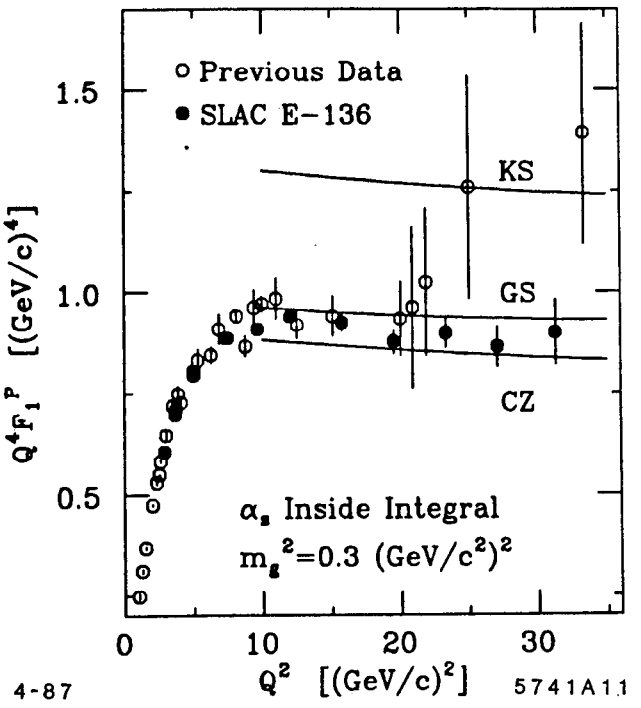

Fig. 5. Comparison of perturbative QCD predictions and data for the proton form factor. The calculation, based on the CZ QCD sum rule distribution amplitude, is from ref. 23. The prediction depends on the use of the running coupling constant as a function of the exchanged gluon momentum. The data are from ref. 24.

Nevertheless, one can question[22] with the consistency of the perturbative QCD analysis, particularly for baryon reactions at moderate momentum transfer:

1. The perturbative analysis of the baryon form factor and large angle hadron-hadron scattering depends on the suppression of the endpoint regions $x_i \sim 1$ and pinch singularity contributions. This suppression occurs automatically in QCD due to Sudakov form factors, as has been shown by Mueller[11] based on the all-orders analysis of the vertex function by Sen.[27] Since these analyses require an all-orders resummation of the vertex corrections, they cannot be derived by standard renormalization group analysis. In this sense the baryon and large angle scattering results are considered less rigorous than the results from analysis of the meson form factor and the $\gamma\gamma$ production of meson pairs.[28]
2. The magnitude of the proton form factor is sensitive to the $x \sim 1$ dependence of the proton distribution amplitude, where non-perturbative effects could be important. The CZ asymmetric distribution amplitude, in fact, emphasizes contributions from the large x region. Since non-leading corrections are expected when the quark propagator scale $Q^2(1-x)$ is small, relatively large Q^2 is required to clearly test the perturbative QCD predictions. A similar criterion occurs in the analysis of corrections to QCD evolution in deep inelastic lepton scattering. Dziembowski and Mankiewicz[19] claim that one can consistently fit low energy phenomena (the nucleon magnetic moments), the measured high momentum transfer hadron form factors, and the CZ distribution amplitudes with a self-consistent ansatz for the quark wavefunctions.

A complete derivation of the nucleon form factors at all momentum transfers would require a calculation of the entire set of hadron Fock wavefunctions. (See fig. 8.) This is the

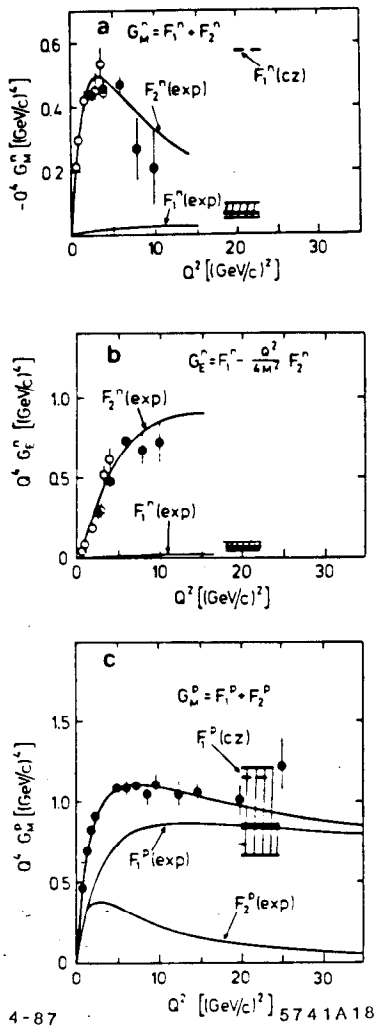

Fig. 6. Predictions for the nucleon form factors assuming VMD at low Q^2 and perturbative QCD at high Q^2. From ref. 25.

goal of the "discretized light-cone quantization" approach[29] for finding the eigen-solutions of the QCD Hamiltonian quantized at equal light cone time $\tau = t + z/c$. using a discrete basis. Thus far results have been obtained for the spectrum and wavefunctions for QED and Yukawa field theories in one-space and one-time dimension. The structure function of the lowest mass bound state in QED[1+1] as a function of a scaled coupling constant is shown in fig. 9.

Color Transparency

The QCD analysis of exclusive processes depends on the concept of a Fock state expansion of the nucleon wavefunction, projected onto the basis of free quark and gluon Fock states. The expansion is done at equal time on the light-cone and in the physical light-cone gauge. At large momentum transfer the lowest particle-number "valence" Fock component with all the quarks within an impact distance $b_\perp \leq 1/Q$ controls the form factor at large Q^2. Such a Fock state component has a small color dipole moment and thus interacts only weakly with hadronic or nuclear matter.[8,9] Thus if elastic electron-scattering is measured as a quasi-elastic process inside a nucleus, one predicts negligible final state interactions in the target as Q becomes large. Integrating over Fermi-motion, one predicts[20] that the differential cross section is additive in the number of nucleons in the nucleus. A test of this novel effect, "color transparency", has recently been carried out at

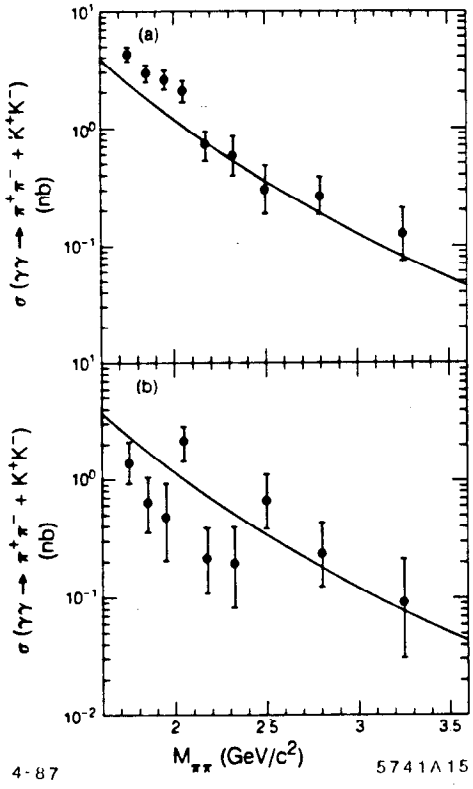

Fig. 7. Measurements[26] of exclusive two-photon reactions compared with the perturbative QCD predictions of ref. 28. The predictions are nearly independent of the shape of the meson distribution amplitudes.

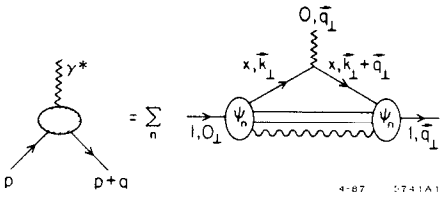

Fig. 8. Representation of electoweak hadron form factors in the light-cone formalism. The sum is over all charged quark lines and all Fock states ψ_n.

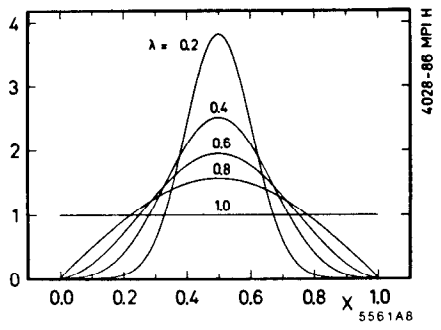

Fig. 9. The structure function of the lowest mass bound state for QED in 1+1 space-time dimensions, as calculated in the DLCQ formalism.[30]

Brookhaven for large momentum transfer elastic pp scattering in nuclear targets by a BNL-Columbia collaboration.[31] The initial results are consistent with diminished absorptive cross sections at large momentum transfer. If these preliminary results are verified they could provide a striking confirmation of the perturbative QCD predictions.

The strong spin-asymmetries seen in elastic p-p scattering[32] and the oscillations of the data modulating the predicted dimensional counting rule power-law fall-off[33] suggest possible resonant interference effects with the perturbative amplitude. [See also ref. 34.] These features evidentially cannot be explained in terms of the simplest QCD perturbative contributions.[35] (See fig. 10.) It is interesting to speculate whether one is observing an interference with pinch singularity contribution[34] or di-baryon resonances associated with the "hidden color" degrees of freedom of the six-quark state.[36] Since the resonant contributions are not coupled to small valence Fock states, one could expect significant final state corrections at energies where the resonances are important. Thus color transparency can be used to distinguish mechanisms for hadron scattering.

In the case of nucleon transition form factors measurable in inelastic electron nucleon scattering, the magnitude of the final state interactions should depend on the nature of the excited baryon. For example final state resonances which are higher orbital qqq states should have large color final state interactions.

Perhaps the most dramatic application of color transparency is to the QCD analysis of the deuteron form factor at large momentum transfer.[20,43] A basic feature of the perturbative QCD formalism is that the six-quark wavefunction at small impact separation controls the deuteron form factor at large Q^2. Thus even a complex six-quark state can have negligible final state interactions in a nuclear target–provided it is produced in a large momentum transfer reaction. One thus predicts that the "transparency ratio" $\frac{d\sigma}{dt}[eA \to ed(A-1)]/\frac{d\sigma}{dt}[ed \to ed]$ will increase with momentum transfer. The normalization of the effective number of deuterons in the nucleus can be determined by single-arm quasi-elastic scattering.

Other experimental tests of the reduced amplitude formalism are discussed in a later section.

Diffractive Electroproduction Channels

As a further example of the richness of the physics of exclusive electroproduction consider the "diffractive" channel $\gamma^* p \to \rho^0 p$. At large momentum transfer, QCD factorization for exclusive amplitudes applies, and we can write each helicity amplitude in the form:[10]

$$M_{\gamma^* p \to \rho^0 p}(s,t,q^2) = \int \prod dx_i \; T_H(x_i, p_T^2, \theta_{cm}, q^2)$$

$$\times \; \phi^\dagger_{\rho^0}(x_i, p_T)\phi^\dagger_p(x_i, p_T)\phi_p(x_i, p_T) \; .$$

This represents the convolution of the distribution amplitudes $\phi(x,Q)$ for the ingoing and outgoing hadrons with the quark-gluon hard scattering amplitude $T_H(\gamma^* + (qqq)_p \to (q\bar{q})_{\rho^0} + (qqq)_p)$ for the scattering of the quarks from the initial to final hadron directions. Since T_H involves only large momentum transfer, it can be expanded in powers of $\alpha_s(Q^2)$. The distribution amplitudes $\phi(x_i, p_T)$ only depend logarithmically on the momentum transfer scale, as determined from the meson and baryon evolution equations. As we discussed above, the functional dependence of the meson and baryon distribution amplitudes can be predicted from QCD sum rules. A surprising feature of the Chernyak and Zhitnitsky analysis[12] of the distribution amplitude of helicity-zero mesons is the prediction of a double-hump shape of $\phi_M(x,Q)$ with a minimum at equal

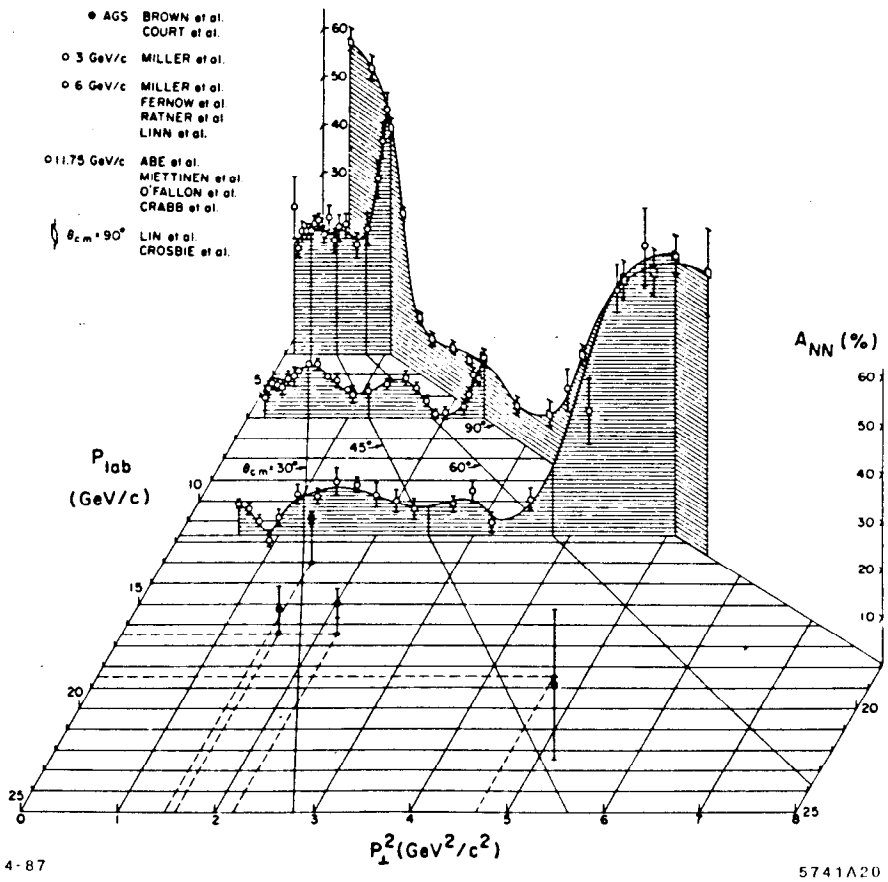

Fig. 10. Spin asymmetry for polarized pp elastic scattering. From ref. 32.

partition of the light-cone momentum fractions. (See fig. 11.) This result has now been confirmed in a lattice gauge theory calculation of the pion distribution amplitude moments by Martinelli and Sachrajda.[37] Similar conclusions also emerge from the wavefunction ansatz of Dziembowski and Mankiewicz.[19]

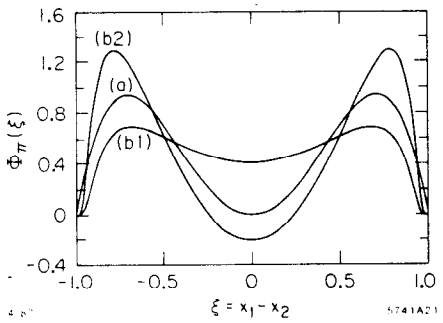

Fig. 11. Theoretical predictions for the pion distribution amplitude.

The main dynamical dependence of the electroproduction amplitude is determined by T_H. To leading order in $\alpha_s(p_T^2)$, T_H can be calculated from minimally-connected tree graphs; power counting predicts

$$T_H = \frac{e\alpha_s^3(p_T^2)}{(p_T^5)}\, f\left(\theta_{cm}, \frac{Q^2}{p_T^2}\right)$$

and thus

$$\frac{d\sigma}{dt}\,(\gamma^* p \to \rho p) \sim \frac{\alpha\alpha_s^6(p_T^2)}{(p_T^2)^7}\, F\left(\theta_{cm}, \frac{Q^2}{p_T^2}\right)$$

to leading order in $1/p_T^2$ and $\alpha_s(p_T^2)$. This prediction is consistent with the dimensional counting rule $d\sigma/dt \sim s^{2-n} f(\theta_{cm})$ where $n = 9$ is the total number of initial and final fields. The scaling laws hold for both real and virtual photons. As shown in fig. 12, the data[38] for $\gamma p \to \pi^+ n$ are consistent with the QCD scaling law prediction.

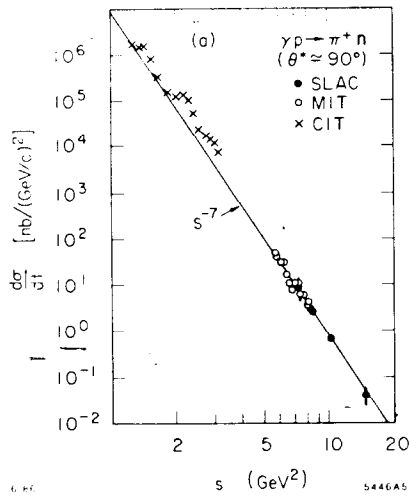

Fig. 12. Comparison of pion photoproduction data[38] at $\theta_{cm} = \pi/2$ with the quark counting rule prediction.

The leading contributions at large momentum transfer in QCD satisfy hadron helicity conservation[17]

$$\lambda_p = \lambda_{p'} + \lambda_\rho\ .$$

This selection rule is an important test of the vector coupling of the gluon in QCD. The result is independent of the photon helicity! Furthermore, the leading behavior comes from the "point-like" Fock component of the photon. The vector-meson-dominance contribution corresponds to the $q\bar{q}$ state where the constituent momenta are restricted to be collinear to the photon. This region gives a power-law suppressed $(1/p_T^2)^8$ contribution to the cross section at fixed θ_{cm}.

The dependence on the photon mass in exclusive electroproduction amplitudes in QCD occurs through the scaling variable Q^2/p_T^2. Thus for $Q^2 \ll p_T^2$, the transverse photon electroproduction amplitudes are predicted to be insensitive to Q^2. This is in striking consequence to the vector meson dominance picture, which predicts a universal $1/(1 + Q^2/m_\rho^2)$ dependence in the amplitude. Furthermore, since only the point-like component of the photon is important at large p_T, one expects no absorption of the initial state photon as it penetrates a nuclear target. The reaction $\gamma^* n \to \pi^- p$ is a particularly interesting test of color transparency since the dependence on photon mass and momentum transfer can be probed.

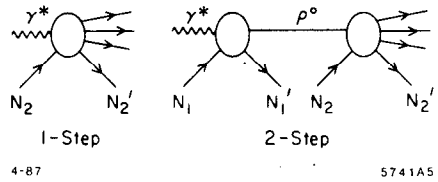

Fig. 13. Conventional description of nuclear shadowing of low Q^2 virtual photon nuclear interactions. The 2-step amplitude is opposite in phase to the direct contribution on nucleon N_2 because of the diffractive vector meson production on upstream nucleon N_1.

The conventional theory[39] of shadowing of photon interactions is illustrated in fig. 13. At large Q^2 the two-step amplitude is suppressed and the shadowing effect becomes negligible. This is the basis for a general expectation that shadowing of nuclear structure functions is actually a higher-twist phenomena, vanishing with increasing Q^2 at fixed x. [A recent analysis on shadowing in electroproduction by Qiu and Mueller[40] based on internucleon interactions in the gluon evolution equation in a nucleus suggests that shadowing is a higher twist effect, but decreases slowly as Q^2 increases.] Thus we predict simple additivity for exclusive electroproduction in nuclei

$$\overline{\frac{d\sigma}{dt}}\,(\gamma^* A \to \rho^0 N(A-1)) = A\,\frac{d\sigma}{dt}\,(\gamma^* N \to \rho^0 N)$$

to leading order in $1/p_T^2$. (The bar indicates that the cross sections are integrated over the nucleon Fermi motion.) This is another application of color transparency. What is perhaps surprising is that the prediction holds for small Q^2, even $Q^2 = 0$! Note that the leading contribution in $1/p_T^2$ (all orders in $\alpha_s(p_T^2)$) comes from the $\gamma \to q\bar{q}$ point-like photon coupling in T_H where the relative transverse momentum of the $q\bar{q}$ are of order p_T. Thus the "impact" or transverse size of the $q\bar{q}$ is $1/p_T$, and such a "small" color dipole has negligible strong interactions in a nucleus. The final state proton and ρ^0 also couple in leading order to Fock components which are small in impact space, again having minimal initial or final state interactions. If this additivity and absence of shadowing is verified, it will also be important to explore the onset of conventional shadowing and absorption as p_T^2 and Q^2 decrease.

. Electroproduction of Diffractive Channels

Exclusive processes such as virtual Compton scattering, $\gamma^* p \to \gamma p$ and ρ^0 electroproduction $\gamma^* p \to \rho^0 p$ play a special role in QCD as key probes of "pomeron" exchange and its possible basis in terms of multiple-gluon exchange.[7] At large photon energy, the diffractive amplitudes are dominated by $J = 1$ Regge singularities.

Recent measurements of $\gamma^* p \to \rho^0 p$ by the EMC group[41] using the high energy muon beam at the SPS show three unexpected features: (1) The ρ^0 is produced with zero helicity at $Q^2 \geq 1$ GeV^2; (2) the falloff in momentum transfer becomes remarkably flat for $Q^2 \geq 5$ GeV^2; and (3) the integrated cross section falls as $1/Q^4$.

The most surprising feature of the EMC data is the very slow fall-off in t for the highest Q^2 data. (See fig. 14.) Using the parameterization $e^{bt'}$, $t' = |t - t_{min}|$, the slope for $7 \leq Q^2 \leq 25$ GeV^2, $E_L = 200$ GeV data is $b \sim 2$ GeV^{-2}. If one assumes Pomeron factorization, then the fall-off in momentum transfer to the proton should be at least as fast as the square of the proton form factor,[42] representing the probability to keep the scattered proton intact. (See fig. 15(b).) The predicted slope for $|t| < 1.5$ GeV^2 is $b \sim 3.4$ GeV^{-2}, much steeper than the EMC data. The background due to inelastic effects is estimated by the EMC group to be less than 20% in this kinematic domain.

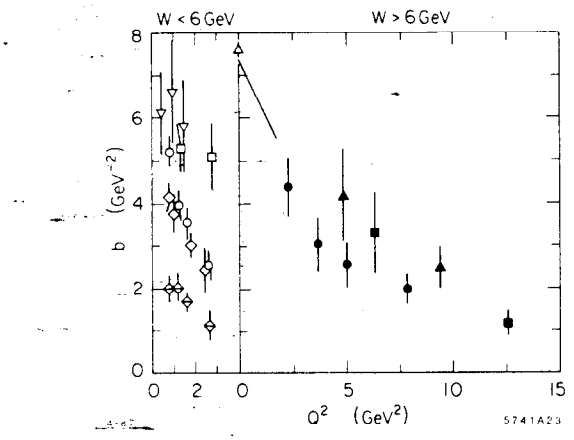

Fig. 14. The slope parameter b for the form $d\sigma/dt = Ae^{bt'}$ fit to the EMC data (ref. 41) for $\mu p \to \mu \rho^0 p$ for $|t'| \leq 1.5$ GeV^2.

In the vector meson dominance picture one expects: (1) dominantly transverse ρ polarization (s-channel helicity conservation); (2) fall-off in t similar to the square of the proton form factor (Pomeron factorization); and (3) a $1/Q^2$ asymptotic fall-off when longitudinal photons dominate.

The physics of electroproduction is quite different in QCD. At large $Q^2 \gg p_T^2$ diffractive channels take on a novel character.[7] (See fig. 15(c).) The transverse momentum k_T in the upper loop connecting the photon and ρ^0 is of order the photon mass scale, $k_T \sim Q$. (Other regions of phase space are suppressed by Sudakov form factors). Thus just as in deep inelastic inclusive scattering, the diffractive amplitude involves the proton matrix element of the product of operators near the light-cone. In the case of virtual Compton scattering $\gamma^* p \to \gamma p'$, one measures product of two electromagnetic currents. Thus one can test an operator product expansion similar to that which appears in deep inelastic lepton-nucleon scattering, but for non-forward matrix elements. In such a case the upper loop in fig. 15(c) can be calculated using perturbative methods. The ρ enters through the same distribution

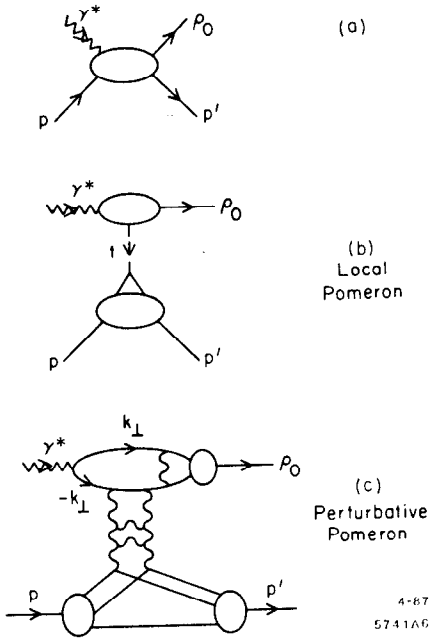

Fig. 15. (a) Diffractive electroproduction of vector mesons. (b) Local pomeron contribution coupling to one quark. (c) Perturbative pomeron contribution. For large transverse momentum $k_t^2 \approx Q^2$ two-gluon exchange contributions are dominant.

amplitude that appears in large momentum transfer exclusive reactions. Since the gauge interactions conserve helicity, this implies $\lambda_\rho = 0$, $\lambda_p = \lambda_p'$ independent of the photon helicity. The predicted canonical Q^2 dependence is $1/Q^4$, which is also consistent with the EMC data.

Since the EMC data is at high energy ($E_\gamma = 200$ GeV, $s \gg p_T^2$) one expects that the vector gluon exchange diagrams dominate quark-exchange contributions. One can show that the virtuality of the gluons directly coupled to the $\gamma \to \rho$ transition is effectively of order Q^2, allowing a perturbative expansion. The effect is a known feature of the higher Born, multi-photon exchange contributions to massive Bethe Heitler processes in QED.[6]

The dominant exchange in the t-channel should thus be the two-gluon ladder shown in fig. 15(c). This is analogous to the diagrams contributing to the evolution of the gluon structure function. If each gluon carries roughly half of the momentum transfer to different quarks in the nucleon, then the fall-off in t can be significantly slower than that of the proton form factor, since in the latter case the momentum transfer to the nucleon is due to the coupling to one quark. This result assumes that the natural fall-off of the nucleon wavefunction in transverse momentum is Gaussian rather than power-law at low momentum transfer.

In the case of quasi-elastic diffractive electroproduction in a nuclear target, we expect neither shadowing of the incident photon nor final state interactions of the outgoing vector meson at large Q^2 (color transparency).

Thus ρ^0 electroproduction and virtual Compton scattering can give essential information on the nature of diffractive (pomeron exchange) processes. Data at all energies and kinematic regions are clearly essential.

Exclusive Nuclear Processes in QCD

One of the most elegant areas of application of QCD to nuclear physics is the domain of large momentum transfer exclusive nuclear processes. Rigorous results have been given by Lepage, Ji and myself[43] for the asymptotic properties of the

deuteron form factor at large momentum transfer. The basic factorization is shown in fig. 16. In the asymptotic $Q^2 \to \infty$ limit the deuteron distribution amplitude, which controls large momentum transfer deuteron reactions, becomes fully symmetric among the five possible color-singlet combinations of the six quarks. One can also study the evolution of the "hidden color" components (orthogonal to the np and $\Delta\Delta$ degrees of freedom) from intermediate to large momentum transfer scales; the results also give constraints on the nature of the nuclear force at short distances in QCD. The existence of hidden color degrees of freedom further illustrates the complexity of nuclear systems in QCD. It is conceivable that six-quark d^* resonances corresponds to these new degrees of freedom may be found by careful searches of the $\gamma^* d \to \gamma d$ and $\gamma^* d \to \pi d$ channels.

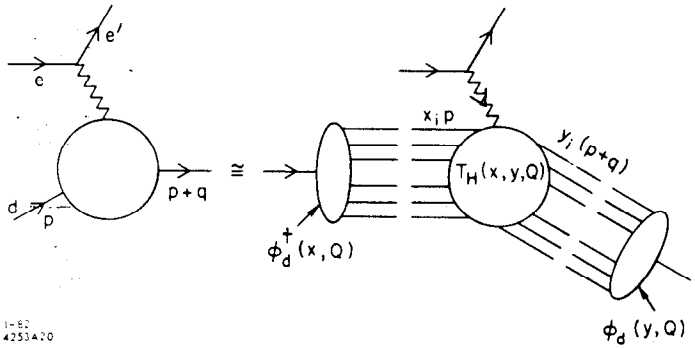

Fig. 16. Factorization of the deuteron form factor at large Q^2.

The QCD analyses suggests a consistent way to eliminate the effects of nucleon compositeness in exclusive nuclear reactions.[20,44] The basic observation is that for vanishing nuclear binding energy $\epsilon_d \to 0$, the deuteron can be regarded as two nucleons sharing the deuteron four-momentum. The $\gamma^* d \to np$ amplitude then contains two factors representing the probability amplitude for the proton and neutron to remain intact after absorbing momentum transfers

$$\hat{t} = \left(p_p - \tfrac{1}{2} p_d\right)^2 \quad \text{and} \quad \hat{u} = \left(p_n - \tfrac{1}{2} p_d\right)^2 .$$

The "reduced" amplitude

$$m_r(\gamma^* d \to np) = \frac{M(\gamma^* d \to np)}{F_{1N}(\hat{t}) F_{1N}(\hat{u})}$$

is predicted to have the same fixed angle scaling behavior as $\gamma^* M \to q\bar{q}$; i.e., the nucleons are reduced to point particles. We thus predict

$$\frac{\frac{d\sigma}{d\Omega_{cm}}(\gamma^* d \to np)}{F_{1N}^2(\hat{t}) F_{1N}^2(\hat{u})} \sim \frac{f(\Omega_{cm})}{(p_T^2)^2}$$

to leading order in $1/p_T^2$.

The analogous analysis (see fig. 17) of the deuteron form factor as defined in

$$\frac{d\sigma}{dt}(\ell d \to \ell d) = \left.\frac{d\sigma}{dt}\right|_{point} |F_d(Q^2)|^2$$

yields a scaling law for the reduced form factor

$$f_d(Q^2) \equiv \frac{F_d(Q^2)}{F_{1N}\left(\frac{Q^2}{4}\right) F_{1N}\left(\frac{Q^2}{4}\right)} \sim \frac{1}{Q^2}$$

i.e., the same scaling law as a meson form factor. As shown in fig. 18, this scaling is consistent with experiment for $Q^2 = p_T^2 \gtrsim 1$ GeV^2. There is also evidence for reduced amplitude scaling for $\gamma d \to pn$ at large angles and $p_T^2 \gtrsim 1$ GeV^2. (see fig. 19). We thus expect similar precocious scaling behavior to hold for $\bar{p}d \to \pi^- p$ and other $\bar{p}d$ exclusive reduced amplitudes. In each case the incident and outgoing hadron and nuclear states are predicted to display color transparency, i.e. the absence of initial and final state interactions if they participate in a large momentum transfer exclusive reaction.

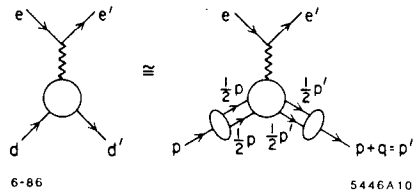

Fig. 17. Application of the reduced amplitude formalism to the deuteron form factor at large momentum transfer.

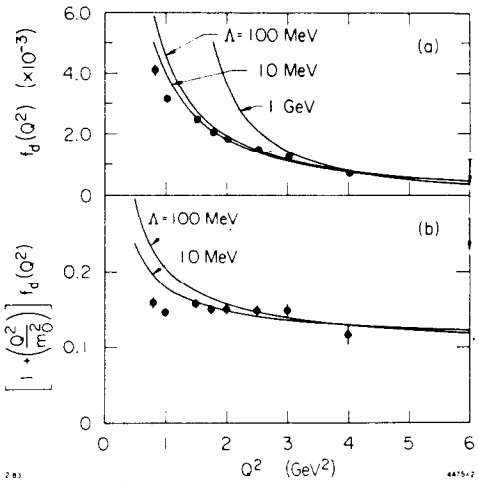

Fig. 18. Scaling of the deuteron reduced form factor. The data are summarized in ref. 20.

Electroproduction: A General View

The factorization formula[45]

$$\frac{d\sigma(AB \to CX)}{d^3p_c/E_c} \cong \sum_{ab,cd} \int_0^1 dx_a \int_0^1 dx_b \int_0^1 \frac{dx_c}{x_c^2}$$

$$\times G_{a/A}(x_a, Q) G_{b/B}(x_b, Q) \tilde{G}_{C/c}(x_c, Q)$$

$$\times \delta(s' + t' + u') \frac{s'}{\pi} \frac{d\sigma}{dt'}(ab \to cd)$$

for the inclusive production processes $AB \to CX$ has general validity in gauge theory. The systems A, B, C can be leptons, photons, hadrons, or nuclei. The primary subprocess in electroproduction is $eq \to eq$. The electron structure function $G_{e/e}(x, Q)$ automatically provides the (leading logarithmic) QED radiative corrections. The energy distribution of the beam itself plays the role of the non-perturbative or initial structure function. (See fig. 20(b).) The subprocess $\gamma^* q \to gq$ corresponds to photon-induced two-jet production. (See fig. 20(a).) This subprocess dominates reactions in which

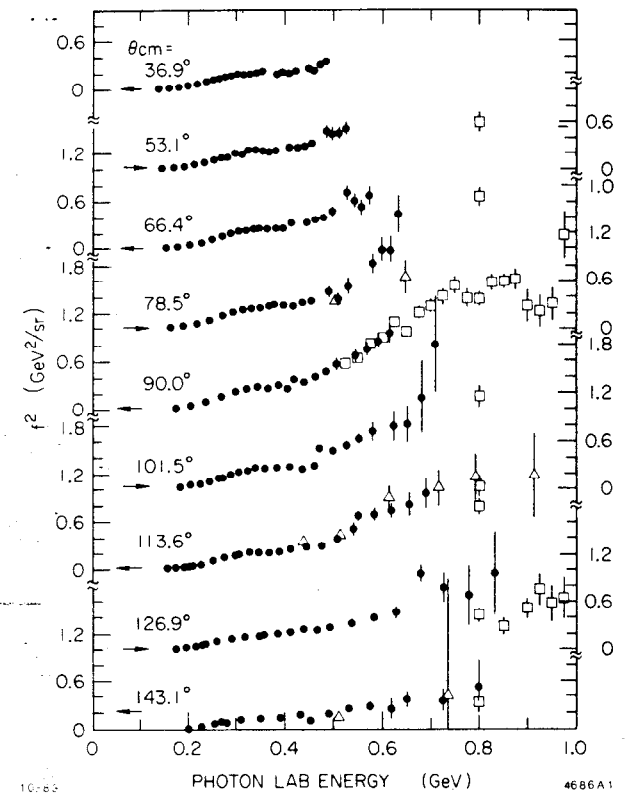

Fig. 19. Scaling of the reduced amplitude for deuteron electrodisintegration. The data are summarized in ref. 44.

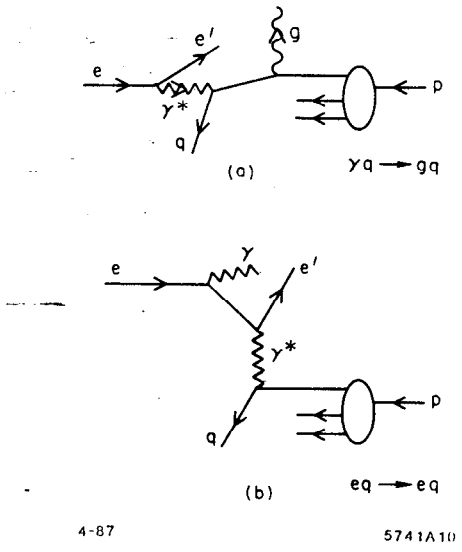

Fig. 20. Application of gauge theory factorization to electroproduction. (a) The $\gamma q \to gq$ subprocess produces hadron jets at high p_T. (b) The $eq \to eq$ produces one quark jet and one recoil electron jet at high p_T. The QED radiative corrections are incorporated into the electron and photon QED structure functions.

the large transverse momentum trigger is a hadron rather than the scattered lepton. Thus one sees that conventional deep inelastic $eq \to eq$ scattering subprocess is just one of the several modes of electroproduction.

The dominant contribution to the meson semi-inclusive cross section is predicted by QCD factorization to be due to jet fragmentation from the recoil quark and spectator diquark jets. When the momentum transfer is in the intermediate range $1 \lesssim Q^2 \lesssim 10$ GeV^2, several other contributions for meson production are expected to become important in $eN \to e'MX$. These include:

(1) Higher twist contributions to jet fragmentation:

$$\frac{dN_\pi}{dz} = D_{\pi/q}(z,Q^2) \cong A(1-z)^2 + \frac{C}{Q^2} \qquad (z \to 1) .$$

The scaling term reflects the behavior of the pion fragmentation function at large fractional momentum ($z \to 1$) as predicted by perturbative QCD (one-gluon exchange). (See fig. 21(a).) The C/Q^2 term[46] is computed from the same perturbative diagrams. For large z where this term dominates, we predict that the deep inelastic cross section will be dominantly longitudinal rather than transverse $R = \sigma_L/\sigma_T > 1$.

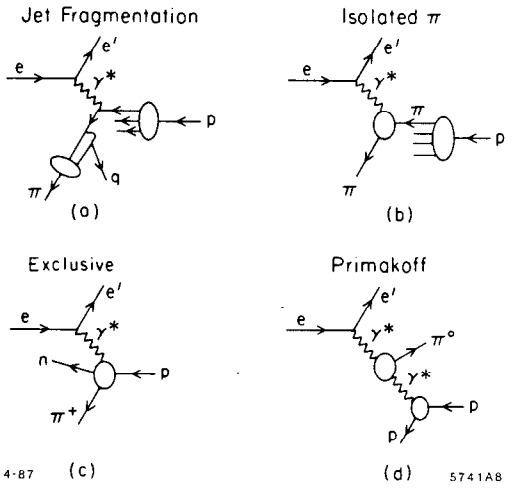

Fig. 21. QCD contributions to pion electroproduction. (a) Jet fragmentation, including leading and $1/Q^2$ higher twist contributions. (b) Isolated pion contributions at order $1/Q^4$. (c) Exclusive production. (d) Primakoff contribution.

(2) "Direct" meson production. Isolated pions may also be created by elastic scattering off of an effective pion current: (See fig. 21(b).)

$$\frac{d\sigma}{dQ^2 dx_\pi} = G_{\pi/p}(x_\pi) \left.\frac{d\sigma}{dQ^2}\right|_{e\pi \to e\pi}$$

$$\left.\frac{d\sigma}{dy dQ^2}\right|_{e\pi \to e\pi} = \frac{4\pi\alpha^2}{(Q^2)^2} |F_\pi(Q^2)|^2 (1-y) .$$

Here $y = q \cdot p / p_e \cdot p$. In the case of a nuclear target, one can test for non-additivity of virtual pions due to nuclear effects, as predicted in models[47] for the EMC effect[41] at small x_{Bj}. Jaffe and Hoodbhoy[48] have shown that the existence of quark exchange diagrams involving quarks of different nucleons in the nucleus invalidates general applicability of the simplest convolution formulae conventionally used in such analyses. The $G_{\pi/p}(x,Q)$ structure function is predicted to behave roughly as $(1-x)^5$ at large x, as predicted from spectator quark counting rules.[15,45] Applications of these rules to other off-shell nucleon processes are discussed in refs. 20 and 49.

(3) Exclusive Channels. (See fig. 21(c).) The mesons can of course be produced in exclusive channels; e.g. $\gamma^* p \to \pi^+ n$, $\gamma^* p \to \rho^0 p$. Pion electroproduction extrapolated to $t = m_\pi^2$ provides our basic knowledge of the pion form factor at spacelike Q^2. With the advent of the perturbative QCD analyses of

large momentum transfer exclusive reactions, predictions can be given over the whole range of large t and Q^2. We discussed some of the features of ρ^0 electroproduction above.

(4) Another possible meson production channel is Primakoff production $\gamma^*\gamma \rightarrow \pi^0$, etc., identifiable from very low target recoil events. (See fig. 21(d).) Such measurements would allow the determination of the $\gamma \rightarrow \pi^0$ transition form factor. This quantity, combined with the QCD analysis of the pion form factor leads to a method to determine the QCD running coupling constant $\alpha_s(Q^2)$ solely from exclusive measurements.[28]

The above examples make it clear that complete final state measurements are necessary for separating the various production channels; detailed study of meson electroproduction can yield valuable information concerning basic issues in QCD.

Higher Twist Contributions to Deep Inelastic Scattering

One of the most difficult aspects of electroproduction phenomenology is the separation of logarithmic scaling violations predicted by QCD evolution from the scale violations induced by power law corrections. The lack of a full understanding of these higher twist terms has prevented the extraction of reliable values of the QCD scale Λ_{QCD} from the data. As we have noted above, shadowing behavior in nuclei is likely associated with higher twist contributions. In addition, it is not clear whether ordinary Regge behavior of the inelastic lepton scattering cross section, which is a valid parameterization at fixed Q^2, persists into the scaling region or whether it is associated with higher twist dynamical effects. The fact that the non-singlet structure functions obey additive sum rules suggests that Regge behavior is absent in leading twist.

In some cases the higher twist effect corresponds to coherent many-particle processes which potentially could be identified by study of the final state. As an example, consider the processes illustrated in fig. 22. At intermediate Q^2 and $x = x_{Bj} \sim 1$ the cross section has the simplified form

$$\frac{d\sigma}{dQ^2 dx} = \frac{4\pi\alpha^2}{Q^4}\left[A(1-x)^3 + B(1-x)\left(\frac{1}{Q^2}\right)^2 + C(1-x)^{-1}\left(\frac{1}{Q^2}\right)^4\right].$$

The three terms correspond to lepton scattering off of one, two, or three quarks, respectively. The power in $1/Q^2$ increases with the number of active quarks: $(Q^2)^{2(n_A-1)}$ The power in $(1-x)$ counts the number of spectators required to stop as $x \rightarrow 1$: $(1-x)^{2n_s-1}$. The "diquark" term gives a large σ_L contribution.[46] The analogous structure in the pion structure function has been confirmed in the Drell-Yan reaction $\pi N \rightarrow \mu^+\mu^- X$ at large x.[46] The relative normalization of the power-law suppressed terms is uncertain, although the model calculations based on tree-graph gluon exchange diagrams performed by Blankenbecler, Gunion, and Nason[50] suggests very large coefficients B and C. If this is true for the physical situation, then the existence of such terms would make it very difficult to isolate the logarithmic corrections to scaling, except at very high momentum transfers–where unfortunately the sensitivity to the numerical value of Λ_{QCD} is small. Internal target experiments may be able to confirm the different contributions by studies of the recoil and spectator systems as functions of Q^2 and x together with separation of σ_L and σ_T.

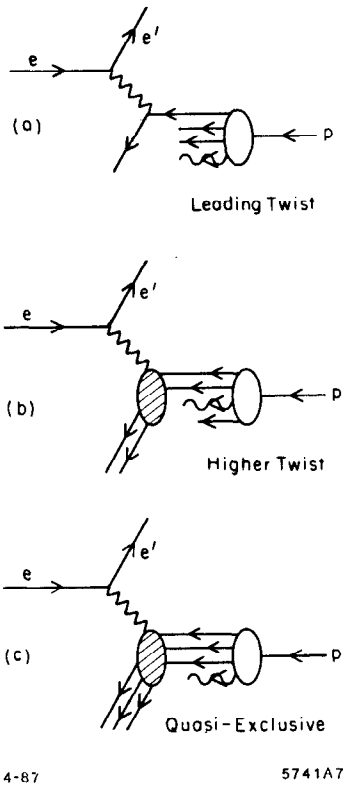

Fig. 22. Leading and higher twist contributions to deep inelastic lepton scattering due to multiparticle hard scattering subprocesses.

Formation Zone Phenomena in Deep Inelastic Scattering

One of the remarkable consequences of QCD factorization for inclusive reactions at large p_T is the absence of inelastic initial or final state interactions of the high energy particles in a nuclear target. Since structure functions measured in deep inelastic lepton scattering are essentially additive (up to the EMC deviations), factorization implies that the $q\bar{q} \rightarrow \mu^+\mu^-$ subprocesses in Drell-Yan reactions occurs with equal effect on each nucleon throughout the nucleus. At first sight this seems surprising since one expects energy loss from inelastic initial state interactions.

In fact, potential inelastic reactions such as quark or gluon bremsstrahlung induced in the nucleus which could potentially decrease the incident parton energy (illustrated in fig. 23) are suppressed by coherence if the quark or gluon energy (in the laboratory frame) is large compared to the target length:

$$E_q > \mu^2 L_A$$

Here μ^2 is the difference of mass squared that occurs in the initial or final state collision. This phenomenon has its origin in studies of QED processes by Landau and Pomeranchuk. The QCD analysis is given by Bodwin, Lepage and myself.[2] Elastic collisions, however, are still allowed, so one expects collision broadening of the initial parton transverse momentum. Recent measurements of the Drell-Yan process $\pi A \rightarrow \mu^+\mu^- X$ by the NA-10 group[51] at the CERN-SPS confirm that the cross section for muon pairs at large transverse momentum is increased in a tungsten target relative to a deuteron target. (See fig. 24). Since the total cross section for lepton-pair production scales linearly with A (aside from relatively small EMC-effect corrections), there must be a corresponding decrease of the ratio

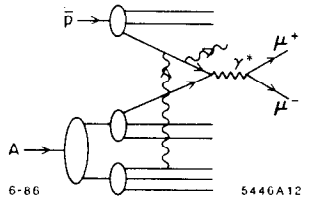

Fig. 23. Induced radiation from the propagation of an antiquark through a nuclear target in massive lepton production. Such inelastic interactions are coherently suppressed at parton energies large compared to a scale proportional to the length of the target.

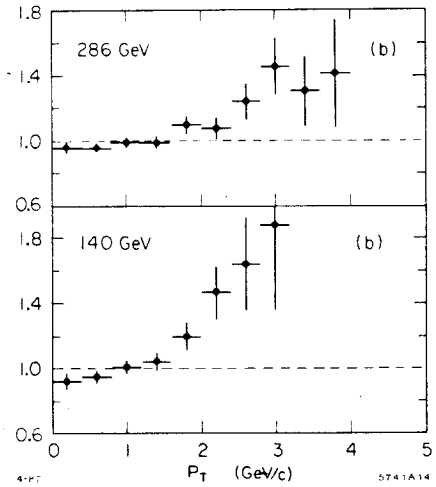

Fig. 24. The ratio $\sigma(\pi^- W \to \mu^+\mu^- X)/\sigma(\pi^- D \to \mu^+\mu^- X)$ as a function of the pair transverse momentum. From ref. 51.

of the differential cross section at low values of the di-lepton transverse momentum. This is also apparent in the data.

These results have striking implications for the interaction of the recoil quark jet in deep inelastic electron-nucleus scattering. For the quark (and gluons) satisfying the length condition, there should be no extra radiation induced as the parton traverses the nucleus. Thus gluon radiation of the type illustrated in fig. 25 should be suppressed. However, low energy gluons, emitted in the deep inelastic electron-quark collision, can suffer radiative losses, leading to cascading of soft particles in the nucleus. It is clearly very important to study this phenomena as a function of recoil quark energy and nuclear size.

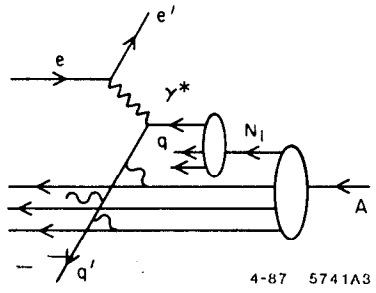

Fig. 25. Propagation of the struck quark through a nuclear target. Induced gluon radiation (inelastic final state interactions) is suppressed at high quark energies. Elastic scattering in the final state however is not suppressed.

It should be emphasized that the absence of inelastic initial or final state collisions for high energy partons does not preclude collision broadening due to elastic initial or final state interactions. The elastic corrections are unitary to leading order in $1/Q$ and do not effect the normalization of the deep inelastic cross section. Thus we predict that the mean square transverse momentum of the recoil quark and its leading particles will increase as $A^{1/3}$.

The transverse momentum of the recoil quark reflects the intrinsic transverse momentum of the nucleon wavefunction. The EMC effect[41] implies that quarks in a nucleus have smaller average longitudinal momentum than in a nucleon. (See fig. 26.) Independent of the specific physical mechanism underlying the EMC effect, the quarks in a nucleus would also be expected to have smaller transverse momentum. This effect can counteract to a certain extent the collision broadening of the outgoing jet.

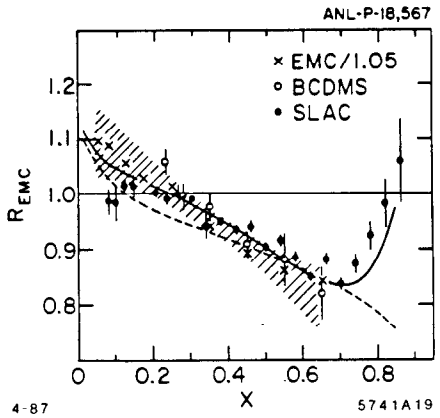

Fig. 26. Ratio of nuclear and nucleon structure functions. The theoretical curves are from the pion current calculation of Berger and Coester, ref. 47.

Unlike the struck quark the remnant of the target system does not evolve with the probe momentum Q. However, since the quantum numbers of the spectator system is $\bar{3}$ in color, nonperturbative hadronization must occur. Since the transverse momentum of the leading particles in the spectator jet is not affected by the QCD radiative corrections, it more closely reflects the intrinsic transverse momentum of the hadron state.

It is also interesting to study the behavior of the transverse momentum of the quark and spectator jets as a function of x_{Bj}. For $x_{Bj} \sim 1$, the 3-quark Fock state dominates the reaction. If the valence state has a smaller transverse size[10] than that of the nucleon, averaged over all of its Fock components, then we expect an increase of $\langle k_\perp^2 \rangle$ in that regime. Evidence for a significant increase of $\langle k_\perp^2 \rangle$ in the projectile fragmentation region at large quark momentum fractions has been reported by the SFM group[52] at the ISR for $pp \to$ dijet $+X$ reactions.

Diffraction Channels and Nuclear Structure Function Non-Additivity

One unusual source of non-additivity in nuclear structure functions (EMC effect) are electroproduction events at large Q^2 and low x which nevertheless leave the nucleus completely intact $x < (1/ML_A)$. In the case of QED, analogous processes such as $\gamma^* A \to \mu^+\mu^- X$ yield nuclear-coherent contributions which scales as $A_{eff} = Z^2/A$. (See fig. 27(a).) Such processes contribute to the Bjorken-scaling, leading-twist cross section.[53] In QCD we expect[54] the nuclear dependence to be less than additive for the analogous gluon exchange contributions (see fig. 27(b)) because of their diffractive coupling to the nucleus. One can identify nuclear-coherent events contributions by observing a rapidity gap between the produced particles and the

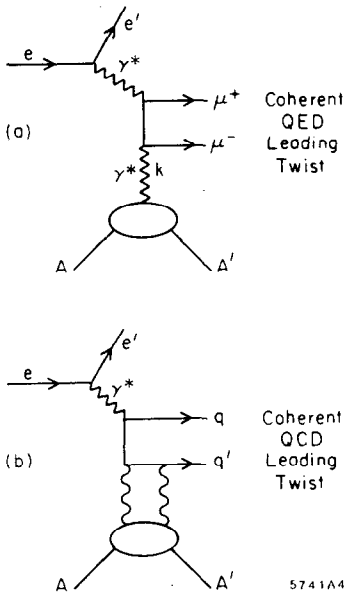

Fig. 27. Leading twist contributions to deep inelastic lepton-nucleus scattering that leave the target intact. (a) QED example. (b) QCD example.

recoiling target. An interesting question is how the gluon momentum fraction sum rule is modified by the diffractive contributions.

Studying "Jet-Coalescence" in Electroproduction

What happens if two jets overlap in phase-space? Certainly independent fragmentation of the jets will fail because of coherent effects. For example, in QED there are strong final state interactions when two charged particles are produced at low relative velocity. In the case of particles of opposite charge $Z_1 e, -Z_2 e$, the QED Born cross sections are corrected by the factor[5] :

$$\sigma = \sigma_0 \frac{2\pi Z_1 Z_2 \alpha / v}{1 - exp(2\pi Z_1 Z_2 \alpha / v)}$$

which increases the cross section dramatically at low relative velocity v. We expect similar effects in QCD when two jets can coalesce to attractive color channels ($Z_1 Z_2 \alpha \to C_F \alpha_s$ for $q\bar{q}$ color singlets). In the case of electroproduction, the low relative velocity enhancements provide a simple estimate of the increase of the $ep \to eX$ cross section at low values of $W^2 = (q+p)^2$, beyond that given by simple duality arguments.

Gunion, Soper and I[6] have recently proposed this jet coalescence mechanism as an explanation of the observed leading particle correlations seen in charm hadroproduction experiments and the anomalously large cross section[55] observed at the SPS for $\Sigma^- N \to A^+(csu)X$ at large x_L. [The hyperon momentum was 135 GeV/c.] In the case of heavy quark electroproduction *e.g.* $\gamma^* g \to s\bar{s}$, $c\bar{c}$, one predicts an enhancement of the cross section when the produced quark is at low rapidity relative to the target fragmentation region. The correction to the rate, integrated over relative rapidity, is found to vanish only as a single inverse power of the heavy quark mass, and thus may give significant corrections to charm production rates and distributions.

Summary

Electroproduction at intermediate energies on an internal target in a storage ring such as PEP could allow the study of many fundamental phenomena in QCD:

(a) A primary goal is the channel-by-channel reconstruction of the final state in electoproduction in order to understand in detail the final state hadronization of both the quark and nucleon spectator jets in a regime where Bjorken scaling is manifest. Such studies can also provide checks on the effect of the higher-twist coherent contributions to electroproduction cross sections. The hadronization of the target jet is a still largely unexplored phenomenon.

(b) The dynamics of individual exclusive electroproduction amplitudes can be probed as a function of all kinematic energy and angle variables including the virtual photon's mass and polarization. As we have discussed here, such processes can often be analyzed systematically in perturbative QCD, providing detailed checks on both QCD dynamics and hadron wavefunctions. The diffractive reactions also allow the study of the non-forward matrix elements of the same operator product entering the near the light-cone analysis of deep inelastic structure functions.

(c) A nuclear target provides a unique probe of short-distance QCD dynamics. The basic subprocesses can be studied in a background nuclear field. In particular, one wants to study the sources of nonadditivity in the nuclear target channel by channel. This includes tests of various shadowing mechanisms, effects of modification of mesonic degrees of freedom, the predicted "color transparency" of quasi-exclusive amplitudes at large momentum transfer inside a nucleus, and the propagation of quark jets through the nuclear medium. Further, as discussed in ref 20, one can use large x measurements to probe nuclear matter in the far off-shell domain. We also note that exclusive channels which involve the scattering of light nuclei at high momentum transfer probe the NN interaction at short distances.

(d) Given sufficient luminosity, internal target experiments could allow the study of strange and charm particle electroproduction near threshold. By comparing electron and positron beam experiments, one can probe[1] virtual Compton scattering; the sum of the quark charges cubed can be obtained from the ratio of the $e^{\pm}p \to e^{\pm}\gamma + X$ cross sections. Polarized proton and nuclear targets allow the study of detailed effects of spin via correlations with final state properties. The combination of polarized target and polarized electron beams allow measurements of the spin dependent structure functions and their sum rules,[56] checks of helicity selection rules, and the separation of different electroproduction channels.

Although there has been extensive of many aspects of electroproduction over the past decade, there are still many phenomena not fully explored. The distinction between logarithmic and power-law scale breaking effects is still in a confused state. Shadowing, diffraction, the interrelation with vector meson dominance, the structure of the (non-evolved) spectator jet system, Regge behavior in non-singlet structure functions, and other phenomena at the boundary between perturbative and non-perturbative effects, all are central topics in hadron and nuclear dynamics, ideally studied in electroproduction.

References

1. S.J. Brodsky, J.F. Gunion and R.L. Jaffe Phys. Rev. **D6**, 2487 (1972).
2. S.J. Brodsky, G.T. Bodwin and G.P. Lepage, in the Proc. of the Volendam Multipart. Dyn. Conf., 1982, p. 841; Proc. of the Banff Summer Inst., 1981, p. 513. This effect is related to the formation zone principle of L. Landau and I. Pomeranchuk, Dok. Akademii Nauk SSSR **92**, 535,735 (1953).
3. G.T. Bodwin, Phys. Rev. **D31**, 2616 (1985); G.T. Bodwin, S.J. Brodsky and G.P. Lepage, ANL-HEP-CP-85-32-mc (1985), presented at 20th Rencontre de Moriond, Les Arcs, France, March 10-17, 1985.
4. E. Berger, ANL-HEP-PR-87-45 and references therein.

5. A. Sommerfeld, *Atombau and Spektallinen* (Vieweg, Braunschweig, 1939).
6. S.J. Brodsky, J.F. Gunion and D. Soper, SLAC-PUB-4193 (1987).
7. S.J. Brodsky and A.H. Mueller, in preparation.
8. A.H. Mueller, Proc. of the Moriond Conf., 1982.
9. S.J. Brodsky, XIII Int. Symp. on Multiparticle Dynamics, 1982.
10. G.P. Lepage and S.J. Brodsky, Phys. Rev. **D22**, 2157 (1980); G.P. Lepage, S.J. Brodsky, T. Huang and P.B. Mackenzie, CLNS-82/522, published in the Proc. of the Banff Summer Institute, 1981.
11. A.H. Mueller, Phys. Rept. **73**, 237 (1981).
12. V.L. Chernyak and I.R. Zhitnitskii, Phys. Rept. **112**, 1783 (1984); Xiao-Duang Xiang, Wang Xin-Nian and Huang Tao, BIHEP-TH-84, 23 and 29 (1984).
13. A.V. Efremov and A.V. Radyushkin, Phys. Lett. **94B**, 245 (1980).
14. S.J. Brodsky, Y. Frishman, G.P. Lepage and C. Sachrajda, Phys. Lett. **91B**, 239 (1980).
15. S.J. Brodsky and G.R. Farrar, Phys. Rev. Lett. **31**, 1153 (1973); Phys. Rev. **D11**, 1309 (1975).
16. S.J. Brodsky and G.P. Lepage, Phys. Rev. **D23**, 1152 (1981); S.J. Brodsky, G.P. Lepage and S.A.A. Zaidi, Phys. Rev. **D23**, 1152 (1981).
17. S.J. Brodsky and G.P. Lepage, Phys. Rev. **D24**, 2848 (1981).
18. I.D. King and C.T. Sachrajda, SHEP-85/86-15 (1986), p. 36.
19. Z. Dziembowski and L. Mankiewicz, Warsaw University preprint (1986).
20. S.J. Brodsky and B.T. Chertok, Phys. Rev. Lett. **37**, 269 (1976); Phys. Rev. **D114**, 3003 (1976).
21. O.C. Jacob and L.S. Kisslinger, Phys. Rev. Lett. **56**, 225 (1986).
22. N. Isgur and C.H. Llewellyn Smith, Phys. Rev. Lett. **52**, 1080 (1984).
23. C-R Ji, A.F. Sill and R.M. Lombard-Nelsen, SLAC-PUB-4068 (1986).
24. R.G. Arnold *et al.*, SLAC-PUB-3810 (1986).
25. M. Gari and N. Stefanis, Phys. Lett. **B175**, 462 (1986); M. Gari and N. Stefanis, preprint RUB-TPII-86-21 (1986).
26. J. Boyer *et al.*, Phys. Rev. Lett. **56**, 207 (1986).
27. A. Sen, Phys. Rev. **D24**, 3281 (1981).
28. S.J. Brodsky and G.P. Lepage, Phys. Rev. **D24**, 1808 (1981). The next to leading order evaluation of T_H for these processes is given by B. Nezic, Ph.D. Thesis, Cornell Univ. (1985).
29. H.C. Pauli and S.J. Brodsky, Phys. Rev. **D32**, 1993 (1985); Phys. Rev. **D32**, 2001 (1985).
30. T. Eller, H.C. Pauli and S.J. Brodsky, Phys. Rev. **D35**, 1493 (1987).
31. S. Heppelmann, DPF Meeting, Salt Lake City (1987).
32. A.D. Krisch, UM-HE-86-39 (1987).
33. A.W. Hendry, Phys. Rev. **D10**, 2300 (1974).
34. J.P. Ralston and B. Pire, Phys. Rev. Lett. **57**, 2330 (1986).
35. S.J. Brodsky, C.E. Carlson and H.J. Lipkin, Phys. Rev. **D20**, 2278 (1979); H.J. Lipkin, private communication.
36. C.-R. Ji and S.J. Brodsky, Phys. Rev. **D34**, 1460; **D33**, 1951; **D33**, 1406; **D33**, 2653 (1986); Phys. Rev. Lett. **55**, 2257 (1985).
37. G. Martinelli and C.T. Sachrajda, CERN-TH-4637/87 (1987). The results are based on the method of S. Gottlieb and A.S. Kronfeld, Phys. Rev. **D33**, 227 (1986); A.S. Kronfeld and D.M. Photiadis, Phys. Rev. **D31**, 2939 (1985).
38. R.L. Anderson *et al.*, Phys. Rev. Lett. **30**, 627 (1973).
39. S.J. Brodsky and J. Pumplin, Phys. Rev. **182**, 1794 (1969); S.J. Brodsky, F.E. Close and J.F. Gunion, Phys. Rev. **D6**, 177 (1972).
40. A.H. Mueller and J. Qui, Nucl. Phys. **B268**, 427 (1986); J. Qui, preprint CU-TP-361.
41. J.J. Aubert *et al.*, Phys. Lett. **123B**, 275 (1983); For a recent review see E.L. Berger and F. Coester, ANL-HEP-PR-87-13 (to be published in Ann. Rev. of Nucl. Part. Sci.).
42. A. Donnachie and P.V. Landshoff, Phys. Lett. **185B**, 403 (1987).
43. S.J. Brodsky, C.-R. Ji and G.P. Lepage, Phys. Rev. Lett. **51**, 83 (1983).
44. S.J. Brodsky and J.R. Hiller, Phys. Rev. **C28**, 475 (1983).
45. J.F. Gunion, S.J. Brodsky and R. Blankenbecler, Phys. Rev. **D8**, 287 (1973); Phys. Lett. **39B**, 649 (1972); D. Sivers, S.J. Brodsky and R. Blankenbecler, Phys. Reports **23C**, 1 (1976). Extensive references to fixed angle scattering are given in this review.
46. E.L. Berger and S.J. Brodsky, Phys. Rev. **D24**, 2428 (1981).
47. E.L. Berger and F. Coester, ANL-HEP-PR-87-13 (1987).
48. P. Hoodbhoy and R.L. Jaffe, Phys. Rev. **D35**, 113 (1987); R.L. Jaffe, CTP #1315 (1985).
49. I.A. Schmidt and R. Blankenbecler, Phys. Rev. **D15**, 3321 (1977).
50. J.F. Gunion, P. Nason and R. Blankenbecler, Phys. Rev. **D29**, 2491 (1984); Phys. Lett. **117B**, 353 (1982).
51. K. Freudenreich, Zurich, NA-10 collaboration.
52. H.G. Fischer, presented at the Leipzig Conference, 1984.
53. G. Alexander, E. Gotsman and U. Maor, Phys. Lett. **161B**, 384 (1985).
54. S.J. Brodsky and M. Soldate, unpublished.
55. S.F. Biagi *et al.*, Z. Phys. **C28**, 175 (1985).
56. R.L. Jaffe, MIT-CTP-1445 (1987).